Use of a liquid crystal display panel as a phase-only spatial light modulator for high order wavefront control

Kuravi Hewawasam[a], Jason Martel[a], Tim Cook[a], Supriya Chakrabarti[a], and Christopher Mendillo[a]

[a]UMass Lowell Center for Space Science and Technology

ABSTRACT

Deformable Mirrors (DMs) that are used in Adaptive Optics applications utilize various technologies such as Voice Coils, Piezoelectric, or Microelectromechanical actuators to manipulate the wavefronts of light. We present a cost-effective alternative for coronagraphic wavefront control using a Liquid Crystal Display (LCD) panel. A transmissive, phase-only Spatial Light Modulator is fashioned out of a monochrome LCD panel, using which we demonstrate Focal Plane Wavefront Control by digging a coronagraphic dark-hole with a Vector Vortex Coronagraph in laser light. We discuss the efficacy of such a device for high-contrast imaging and discuss avenues of improvement.

Keywords: Wavefront Control, Speckle Nulling, Liquid Crystal Display, Spatial Light Modulators, Coronagraphy, High-Contrast Imaging

1. INTRODUCTION

The ever-growing catalog of exoplanets[1] has attracted many toward the field of exo-astronomy: i.e. the science of celestial bodies that orbit stars other than the sun. It is believed that these extra-solar planets and extra-zodiacal debris disks may hold the answers to the questions of our own origin as well as fate.[2–4] Recent studies have confirmed thousands of these exoplanets via various methods of observations, such as astrometry, radial velocity, transit, microlensing, direct imaging etc. Direct imaging of these extremely faint exoplanets and exozodiacal disks next to their bright host stars requires extremely precise manipulation of light in those imaging systems. All direct imaging experiments consists of a coronagraph to block the host starlight. A Coronagraph is an instrument that consists of one or more elements that selectively block or attenuate the starlight making it possible to observe its vicinity that would otherwise be drowned out due to the host starlight. Even for an ideal optical system the fundamental principles of diffraction prevent imaging and distinguishing objects at low angular separations. For real-world telescopes with finite apertures, optical irregularities and detectors with finite dynamic ranges, it is easy to overwhelm the system with the brightness of the star under observation. There is a wide variety of coronagraphs that exploit various properties of light to selectively suppress starlight.[5] A coronagraph's ability to suppress starlight is quantified in terms of contrast and its performance is measured by the coronagraph's contrast at a given angular separation from the observed star. Higher starlight suppression at smaller angular separations allows us to probe closer to a star revealing fainter exo-targets. It has been demonstrated that an earth-like planet orbiting a sun-like star at a distance of 1 au observed from a distance of 1 pc will be 10^9 times fainter than the host star at $1''$ angular separation.[6] The performance of a coronagraph is closely related the quality of the wavefronts of light it is used with. An ideal telescope will be able to utilize a coronagraph at its optimal design parameters. Therefore, a coronagraphic system is usually accompanied by an adaptive optics system that consists of one or more DMs and Wavefront Sensors (WFSs) which are used to correct both dynamic and static errors in the system bringing it closer to the ideal. Adaptive optics that are available to these coronagraphic systems enable special wavefront manipulation techniques that can further improve the contrast of selected regions of the field of view of the instrument by making trade offs in other regions of its field of view.

Further author information: (Send correspondence to K.H.)
K.H.: E-mail: kuravi_hewawasam@uml.edu, Telephone: 1 978 934 4960
C.M.: E-mail: christopher_mendillo@uml.edu, Telephone: 1 978 934 4980

Techniques and Instrumentation for Detection of Exoplanets XII, edited by Garreth J. Ruane, Maxwell A. Millar-Blanchaer, Proc. of SPIE Vol. 13627, 136270Y
2025 Published by SPIE · 0277-786X · doi: 10.1117/12.3063953

Direct imaging of exo-targets pose a challenge that interests many professionals and hobbyists alike. With space coronagraph missions like the Nancy Grace Roman Space Telescope (NGRST) on the horizon the interest of high contrast imaging is bound to increase in the coming years.[7] However access to research in high-contrast imaging is limited due to the cost of these extremely precise optical systems. With DMs being one of the most expensive components of a typical high-contrast imaging testbed, exploring cost effective alternatives could increase access to research in education as well as amateur astronomy.

1.1 DMs and Spatial Light Modulators (SLMs) primer

A DM manipulates the wavefront by changing the shape of a reflective surface which in turn changes the optical path length of the light that reflects off of it. These Micro-Electromechanical Systems (MEMS) consists of arrays actuators that physically move in response to an electrical signal applied to them. Digital Micromirror Devices (DMMs) are binary DMs with actuators with two states but the term DM is usually associated with DMs that have actuators with analog control over their displacement perpendicular to its surface. A DMs actuators maybe piezoelectric, electromagnetic or electrostatic.

SLMs are optical devices that can also modulate the amplitude, phase, or polarization of light across a 2D surface. Typically consisting of pixels similar to the actuators of a DM, an SLM can be reflective (Liquid Crystal on Silicon) or transmissive (Liquid Crystal). While phase only SLMs are dedicated scientific applications, intensity SLMs has found its way to everyday consumer electronics in the form of display devices. Both SLMs and ubiquitous LCDs utilize the electro-optic phenomenon known as the Fréedericksz transition in Liquid Crystal (LC) material to induce phase variation.[8] This effect refers to the field-induced reorientation of LC molecules.

Due to their operational similarities we set out to investigate if a commercial off the shelf (COTS) LCD can can be repurposed as a phase only spatial light modulator for coronagraphic applications. Previous attempts to use an LCD for similar experiments can be found in literature.[9–11] However, using an LCD beyond its intended purpose requires some reverse engineering and measurement of specifications that are not well documented. An LCD consists of an array of LC cells (pixels) sandwiched between two crossed linear polarizers. A single pixel of an LCD is illustrated in Fig. 1a. The LC rotates the linear polarization between the two crossed linear polarization axes as response to an electrical signal. In the fully opaque state, the LC does not alter the polarization state light after the input polarizer. In the fully transmissive state, the LC rotates polarization state of light after the input polarizer to align with the output polarizer analogous to a waveplate. If the LC rotates the input linearly polarized light by 90°, the intensity of the transmitted light will be maximized hence the contrast ratio between the fully opaque state of the pixel to the fully transmissive state of the pixel will be maximized. However it is not necessary for the LC to be a complete half-wave plate. Any rotation of the input polarization induced by the LC will produce an intensity response. Let us approximate the LC layer by a variable wave-plate and in these proceedings we attempt to use this variable wave-plate to control the phase of monochromatic laser light.

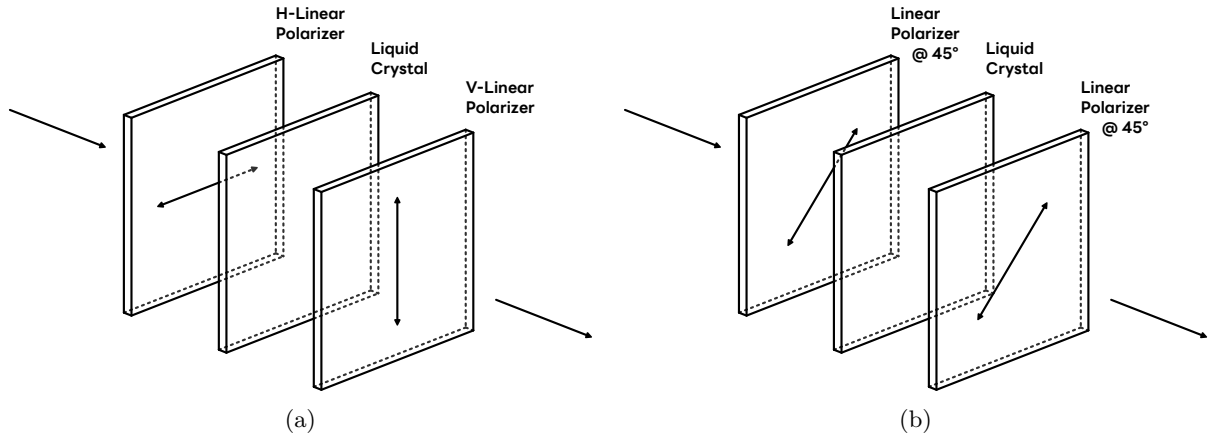

(a) (b)

Figure 1: (a) An LCD pixel is an LC cell sandwiched between two linear polarizers. (b) A phase only SLM is fashioned by re-orienting both linear polarizers 45° to the original input polarizer.

2. THEORY

Disregarding internal structure and focusing on the functional behavior, the LCD can be modeled using Jones calculus as follows. Without loss in generality we may consider the input polarizer to be oriented horizontally and the output polarizer to be oriented vertically. The Jones matrix of a linear polarizer at an arbitrary angle θ can be written as,

$$LP(\theta) = \begin{bmatrix} \cos^2\theta & \cos\theta\sin\theta \\ \cos\theta\sin\theta & \sin^2\theta \end{bmatrix}$$

The Jones matrix of an arbitrary birefringent material can be written as,

$$VPR(\theta,\eta,\phi) = e^{-i\eta/2}\begin{bmatrix} \cos^2\theta + e^{i\eta}\sin^2\theta & (1-e^{i\eta})e^{-i\phi}\cos\theta\sin\theta \\ (1-e^{i\eta})e^{i\phi}\cos\theta\sin\theta & \sin^2\theta + e^{i\eta}\cos^2\theta \end{bmatrix}$$

Where θ is the angle of its fast axis w.r.t the x-axis and $\eta = \phi_x - \phi_y$ is the relative phase retardation between two orthogonal axis. ϕ is the circularity. The compound Jones matrix for the LCD ($LCD(\eta)$) may be written as a product of $LP(\theta+\pi/2)$, $VPR(\theta+\pi/4,\eta,\phi)$ and $LP(\theta)$. With $\theta = 0$ (i.e. horizontal input polarizer);

$$LCD(\eta) = LP(\pi/2)\cdot VPR(\pi/4,\eta,\phi)\cdot LP(0)$$

Passing unpolarized light through this system the first input polarizer will linearly polarize the input light to align with itself. Let us denote light right after the input polarizer as E_{in},

$$E_{in} = \begin{bmatrix} 1 \\ 0 \end{bmatrix}$$

Therefore, the transmitted light can be written as,

$$LCD(\eta)\cdot E_{in} = LP(\pi/2)\cdot VPR(\pi/4,\eta,\phi)\cdot LP(0)\cdot E_{in} = -ie^{i\phi}\sin(\eta/2)\begin{bmatrix} 0 \\ 1 \end{bmatrix} = E_{out} \tag{1}$$

Assuming the LC as a purely linear retarder ($\phi = 0$);

$$E_{out} = -i\sin(\eta/2)\begin{bmatrix} 0 \\ 1 \end{bmatrix} \tag{2}$$

Similarly, the compound Jones matrix for the SLM ($SLM(\eta)$) may be written as a product of $LP(\theta+\pi/4)$, $VPR(\theta+\pi/4,\eta,\phi)$ and $LP(\pi/4)$. Again with $\theta = 0$ (i.e. horizontal input polarizer);

$$SLM(\eta) = LP(\pi/4)\cdot VPR(\pi/4,\eta,\phi)\cdot LP(\pi/4)$$

The transmitted light can be written as,

$$SLM(\eta)\cdot E_{in} = LP(\pi/4)\cdot VPR(\pi/4,\eta,\phi)\cdot LP(\pi/4)\cdot E_{in} = (\cos(\eta/2) - i\cos(\phi)\sin(\eta/2))\begin{bmatrix} 1 \\ 1 \end{bmatrix} = E_{out} \tag{3}$$

The intensity throughput response is a constant, and the bulk phase response is a function of η and ϕ. Again assuming the LC as a purely linear retarder ($\phi = 0$);

$$E_{out} = e^{-i\eta/2}\begin{bmatrix} 1 \\ 1 \end{bmatrix} \tag{4}$$

Fig. 2 illustrates the phase and intensity variations of these two configurations as a function of η. In practice, the η is the command variable, or the value of each pixel of the SLM. Therefore, the phase is varied by setting the value of each pixel. Even though this model implies that LCD intensity should vary as a $\sin^2(\eta/2)$ the control electronics may be calibrated such that the intensity response is linear.

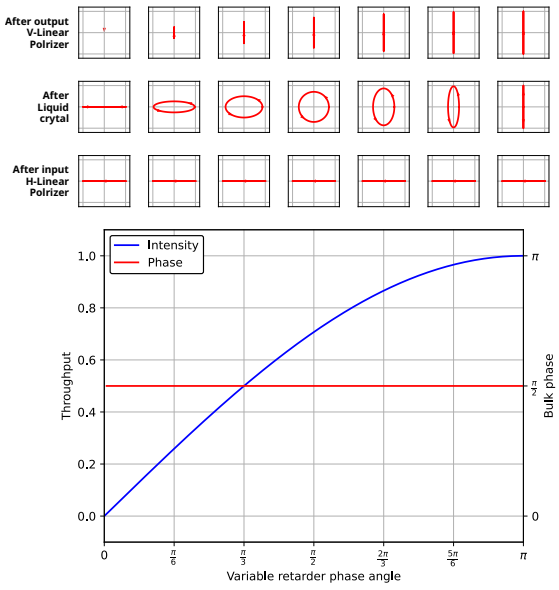

(a)

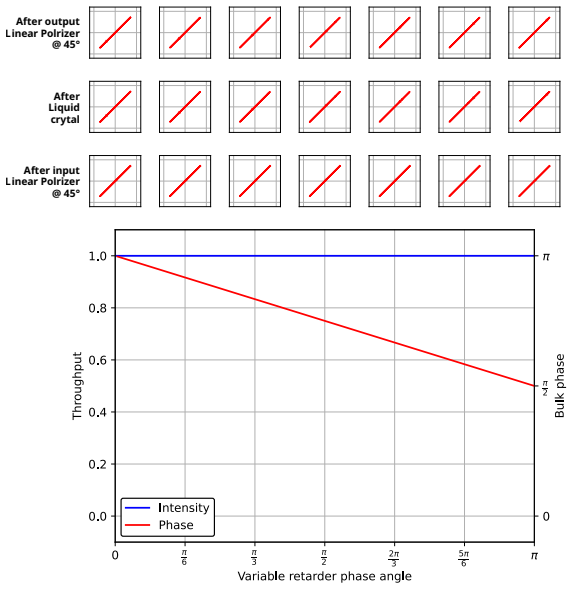

(b)

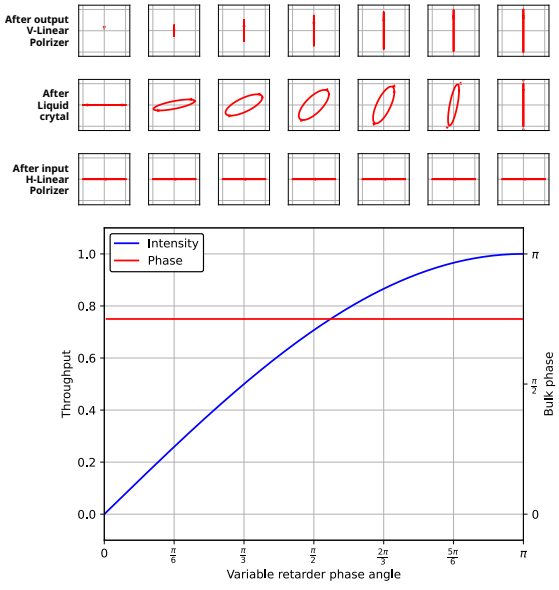

(c)

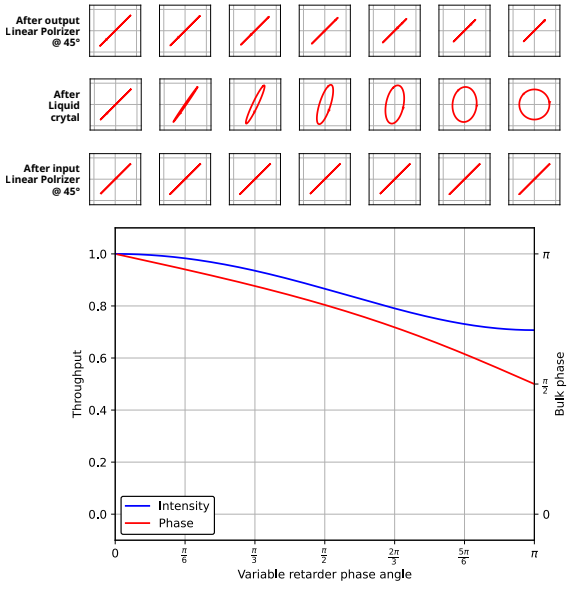

(d)

Figure 2: The intensity and phase responses of the two configurations (a) LCD (Eq. 2) (b) SLM (Eq. 4) for purely linear retarders ($\phi = 0$). Same responses for the two configurations (c) LCD (Eq. 1) (d) SLM (Eq. 3) for a more general elliptic retarder where $\phi = \pi/4$.

3. IMPLEMENTATION

The LCD used in this work is a TFT panel (Part No: RV059FBB-N80[12]) by BOECD Optoelectronics Technology Cooperation. Relevant specifications are listed in Tab. 1. A magnified view of this monochrome LCD pixels are shown in Fig. 3. It was apparent that the fill factor is lower than provided in the vendor's specifications. The LCD is modified by removing the polarizing films and placing it between two linear polarizers angled 45° to the removed films as illustrated in Fig. 1. This configuration will be referred to as the LCD SLM in the rest of this article. Since this application focuses on the phase response of the LCD in this particular configuration, phase measurements were made using Differential Optical Transfer Function (DOTF) wavefront sensing.[13]

Table 1: Relevant specification of the LCD panel RV059FBB-N80.

Parameter	Specification
Active area (H×V)	81 mm × 128 mm
Number of pixels (H×V)	1620 × 2560
Pixel pitch (H×V)	50 µm × 50 µm
Dimensions (H×V×D)	84.6 mm × 135.85 mm × 1.08 mm
Contrast Ratio	∼ 800
Transmittance (for $\lambda = 405$ nm)	∼ 6.4
Response time	35 ms
Refresh rate	60 Hz

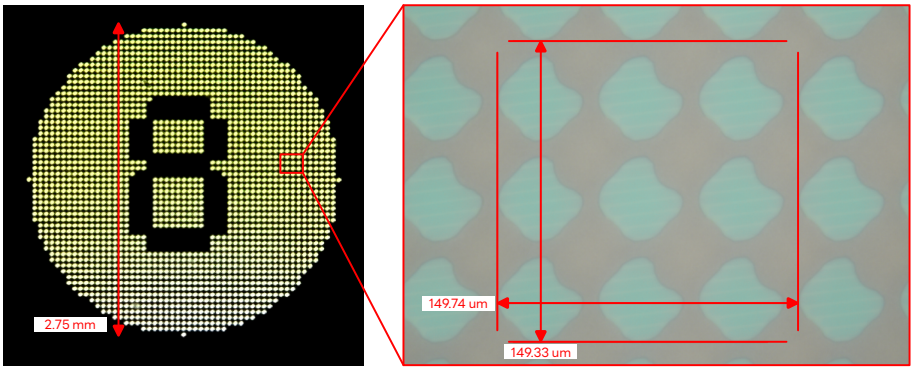

Figure 3: The monochrome LCD panel under the microscope. Unlike a color LCD panel where each pixel consists of three rectangular RGB sub-pixels the monochrome LCD pixels are mostly square in aspect. Each pixel is ∼50 µm in size. Video 1. http://dx.doi.org/10.1117/12.3063953.1

3.1 Phase control using the Spatial Light Modulator

LC SLMs have been widely used in structured light applications.[14] However, recent studies have found that SLMs may also be suitable for wavefront control in coronagraphic applications.[15–17] The commands patterns shown in Fig, 4 were placed on the LCD SLM and the induced phase was measured by calculating the DOTF of the images acquired from the following focal plane. DOTF maps of the five commands are shown on Fig. 5 . The cross sections of the the DOTF maps (Fig. 6) show a clear phase response to each command. Based on the model formulated in Sec. 2, the modified LCD should induce a phase only response if the LC acts as a linear retarder where the circularity (ϕ) is 0. However, DOTF maps display a coupled phase and intensity response suggesting that the LC is more of an elliptical retarder than a linear one (Fig. 2d), which in turn suggests that neither of these responses are linear. It can also be observed that an elliptical retarder have little effect on intensity

variation of the LCD (Compare Figures 2a and 2c). Therefore, it can be assumed that LCD manufacturing process does not take in to account the ellipticity of the LC material. It may also be possible to measure this ellipticity across the panel using a similar DOTFs maps.

Figure 4: Five commands with the maximum set to 0.0, 0.25, 0.5, 0.75 and 1.0, where 1.0 corresponds to the full scale of the LCD SLM.

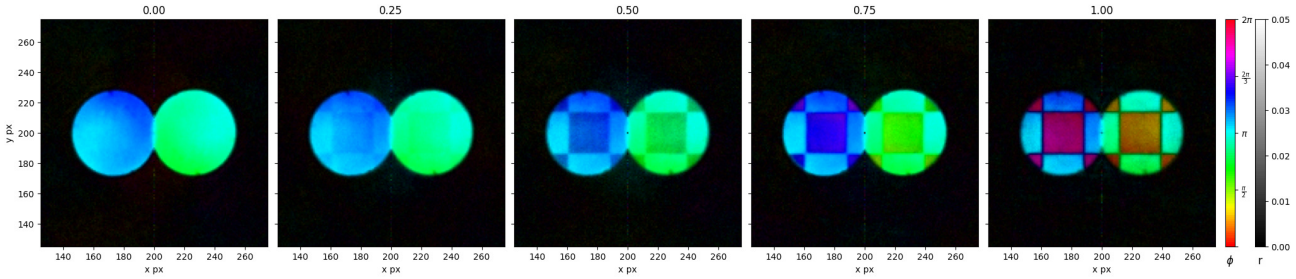

Figure 5: The response DOTF wavefronts for each of the five commands (averaged over 500 measurements).

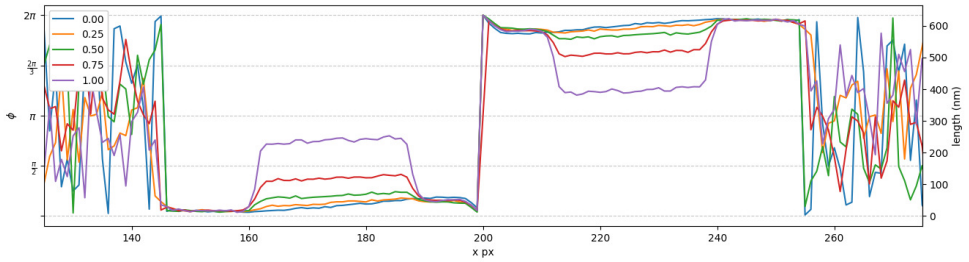

Figure 6: Cross sections of each DOTF map.

3.2 High-Contrast imaging setup

A rudimentary testbed was setup using mostly COTS components to test the SLM wavefront control. Fig. 7 shows the testbed layout. All components (Tab. 2) except for the Vector Vortex Coronagraph (VVC) and the collimator are COTS parts from the vendor Thorlabs. The coronagraph used is a charge 6 VVC in a f/33.3 beam. The LCD SLM is located in a pupil plane and a pupil camera located after the Lyot stop is used for alignment. The beam diameter at the LCD SLM is 9 mm (i.e. 180 pixels). Once the optics are laid out it is crucial to clock the polarizers such that they are aligned as illustrated in Fig. 1b. The following procedure was followed obtain the correct clocking. During the removal of the polarizing films from the LCD the polarizer angles should be identified. When placing the first linear polarizer of the LCD SLM it should be place orthogonal to the removed polarizing film. Then all polarizers and waveplates of the system are removed except for the two linear polarizer before and after the LCD SLM. A command pattern is applied to the LCD SLM and the second polarizer is clocked such that the intensity response on the pupil camera is minimal (see Fig. 8). This procedure guarantees that the two linear polarizers are aligned to the axis of the liquid crystal as well as to each other. The test bed operates on 633 nm monochromatic laser light.

After setting up the testbed, the focal plane algorithm speckle nulling[18] was run on it using the science camera for focal plane imaging and the LCD SLM for pupil plane command actuation.

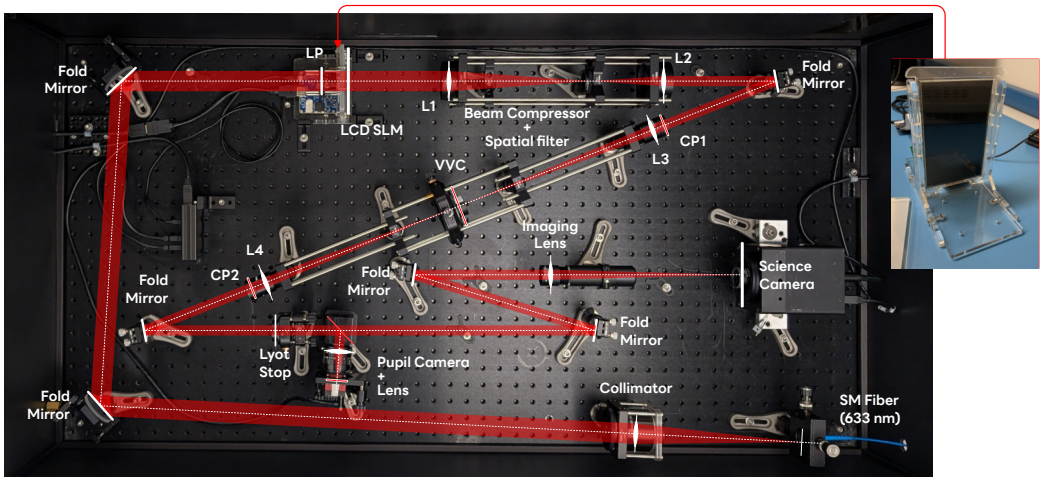

Figure 7: Layout of the coronagraph.

Table 2: All Components of the testbed (except for the VVC) are COTS components.

Designator	Part Number	Description
Laser	HRS015B	Stabilized HeNe Laser, 632.992 nm (Vacuum), 1.2 mW Polarized
Collimator	-	BUHL 9.5" f/4.5 Projector Lens
LP	-	Linear polarizer
LCD SLM	RV059FBB-N80	LCD with polarizing films removed
L1	AC508-200-A-ML	$f = 200$ mm, ⌀ 2" Achromatic Doublet
L2	ACT508-100-A-ML	$f = 100$ mm, ⌀ 2" Achromatic Doublet
CP1	CP1R633	Right-Handed Circular Polarizer, 633 nm
L3	AC254-300-A-ML	$f = 300$ mm, ⌀ 1" Achromatic Doublet
VVC	V600-BB20-Q3-BL	Charge 6 Vector Vortex Coronagraph
L4, Imaging lens	AC254-300-A-ML	$f = 300$ mm, ⌀ 1" Achromatic Doublet
CP2	CP1L633	Left-Handed Circular Polarizer, 633 nm
Lyot stop	-	-
pupil camera	Alvium 1800 U-291m	USB camera with Sony IMX421
Imaging lens	AC254-300-A-ML	$f = 300$ mm, ⌀ 1" Achromatic Doublet
Science camera	FLI MLx694	USB camera with ICX694AL

4. RESULTS AND DISCUSSION

Fig. 9 shows the focal plane speckle field at the start and at the end of ∼270 iterations of speckle nulling. The testbed consistently converged to a mean dark hole contrast of 6.05×10^{-5} within that time (∼1 h Fig. 10). Despite the significant shortcomings of the rudimentary testbed layout this system was still able to produce a dark hole.

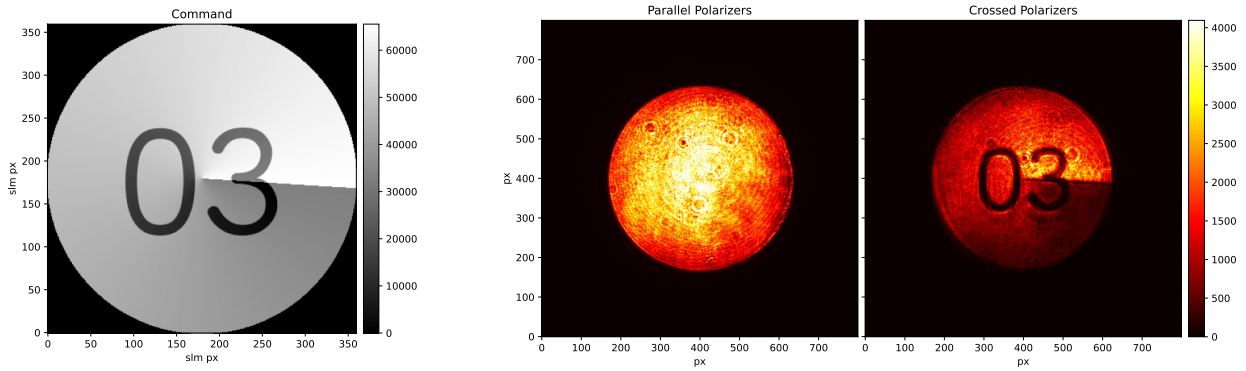

(a) (b)

Figure 8: The LCD SLM command (a) imaged from the pupil camera with polarizers parallel to the fast axis (Fig. 1b) and with polarizers perpendicular to the fast axis (Fig. 1a).

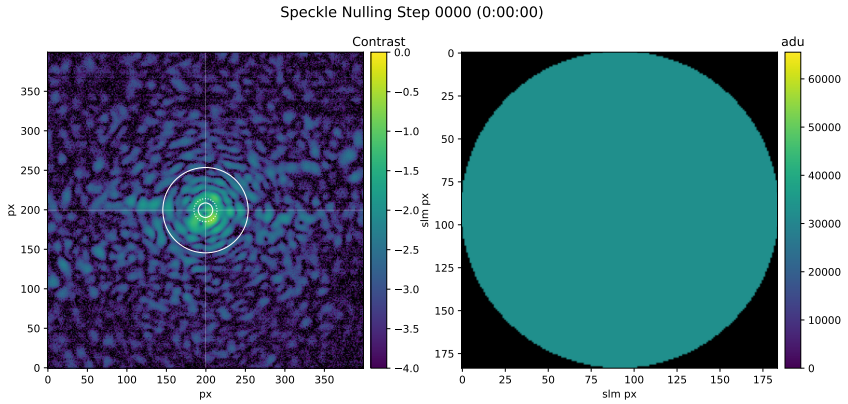

(a)

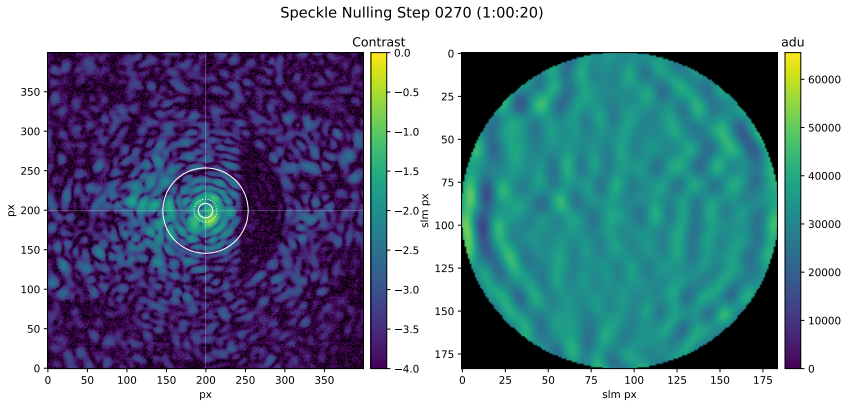

(b)

Figure 9: The system at the start (a) and at the end (b) of 1000 iterations of speckle nulling. The left panels show the image plane speckle field. The three circles correspond to 1.7 λ/d, 2.7 λ/d, 10.0 λ/d. The right panels show the command on the LCD SLM. Video 2. http://dx.doi.org/10.1117/12.3063953.2

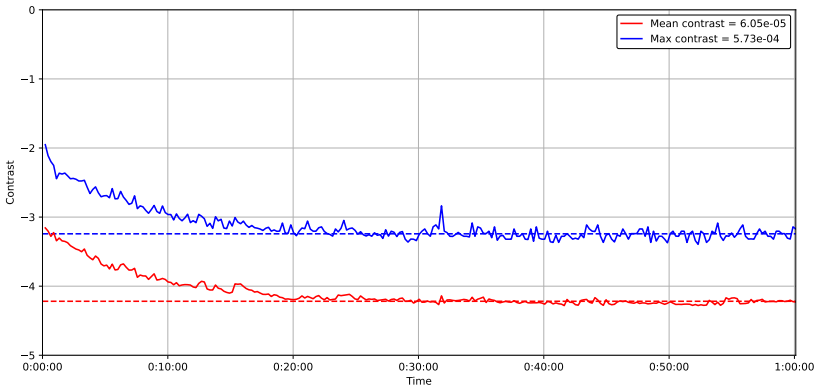

Figure 10: Evolution of contrast over 270 speckle nulling iterations over a duration of 1 h.

Further work would be necessary decouple the intensity variation from the phase variation. Or conversely the coupled intensity and phase variation maybe measured and included in the wavefront control mechanism. Testing broadband performance is also useful for this configuration. Since the LCD SLM is a transmissive element chromaticity will also need to be addressed. It would also be of interest to test other High order wavefront sensing and control mechanisms such as Electric Field Conjunction (EFC) on this system. However, due to the availability of these LCDs we believe that this work would be useful as a demonstration tool in outreach settings or and instructional tool in classroom settings.

ACKNOWLEDGMENTS

This work was partially supported by NASA grant 80NSSC22K1648 along with University of Massachusetts Lowell funds.

REFERENCES

[1] "NASA Exoplanet Archive." exoplanetarchive.ipac.caltech.edu. (Accessed: 2025-08-03).

[2] Hughes, A. M., Duchêne, G., and Matthews, B. C., "Debris Disks: Structure, Composition, and Variability," *Annual Review of Astronomy and Astrophysics* **56**, 541–591 (Sept. 2018).

[3] Matthews, B. C. and Kavelaars, J. J., "Insights into planet formation from debris disks: I. The solar system as an archetype for planetesimal evolution," *Space Science Reviews* **205**, 213–230 (Dec. 2016).

[4] Raymond, S. N., Armitage, P. J., Moro-Martín, A., Booth, M., Wyatt, M. C., Armstrong, J. C., Mandell, A. M., Selsis, F., and West, A. A., "Debris disks as signposts of terrestrial planet formation," *Astronomy & Astrophysics* **530**, A62 (June 2011).

[5] Ruane, G., Riggs, A., Mazoyer, J., Por, E. H., N'Diaye, M., Huby, E., Baudoz, P., Galicher, R., Douglas, E., Knight, J., Carlomagno, B., Fogarty, K., Pueyo, L., Zimmerman, N., Absil, O., Beaulieu, M., Cady, E., Carlotti, A., Doelman, D., Guyon, O., Haffert, S., Jewell, J., Jovanovic, N., Keller, C., Kenworthy, M. A., Kühn, J., Miller, K., Sirbu, D., Snik, F., Wallace, J. K., Wilby, M., and Ygouf, M., "Review of high-contrast imaging systems for current and future ground- and space-based telescopes I. Coronagraph design methods and optical performance metrics," in [*Space Telescopes and Instrumentation 2018: Optical, Infrared, and Millimeter Wave*], 98 (Aug. 2018).

[6] Seager, S., [*Exoplanets*], The University of Arizona Space Science Series, University of Arizona Press (2011).

[7] Bailey, V. P., Bendek, E., Monacelli, B., Baker, C., Bedrosian, G., Cady, E., Douglas, E. S., Groff, T., Hildebrandt, S. R., Kasdin, N. J., Krist, J., Macintosh, B., Mennesson, B., Morrissey, P., Poberezhskiy, I., Subedi, H. B., Rhodes, J., Roberge, A., Ygouf, M., Zellem, R. T., Zhao, F., and Zimmerman, N. T., "Nancy Grace Roman Space Telescope Coronagraph Instrument Overview and Status," (Sept. 2023).

[8] Fréedericksz, V. and Zolina, V., "Forces causing the orientation of an anisotropic liquid," *Trans. Faraday Soc.* **29**(140), 919–930 (1933).

[9] Xiao, X. and Voelz, D., "Jones matrix model with field angle effects for a liquid crystal variable retarder," in [*Polarization Science and Remote Sensing II*], **5888**, 444–452, SPIE (2005).

[10] Villalobos-Mendoza, B., Granados-Agustín, F., Aguirre-Aguirre, D., and Cornejo-Rodríguez, A., "Liquid crystal display for phase shifting," in [*8th Iberoamerican Optics Meeting and 11th Latin American Meeting on Optics, Lasers, and Applications*], **8785**, 822–826, SPIE (2013).

[11] Hu, L., Xuan, L., Liu, Y., Cao, Z., Li, D., and Mu, Q., "Phase-only liquid crystal spatial light modulator for wavefront correction with high precision," *Optics express* **12**(26), 6403–6409 (2004).

[12] "RV059FBB-N80 Specification & Datasheets - Panelook.com." https://www.panelook.com/RV059FBB-N80_BOE_5.9_CELL_parameter_46880.html. (Accessed: 2025-08-03).

[13] Codona, J. L., "Differential OTF Wavefront Sensing," *Optical Engineering* **52**, 097105 (Sept. 2013).

[14] Rosales-Guzmán, C. and Rodriguez-Fajardo, V., "Structured Lightś Applications: A perspective," (Oct. 2024).

[15] Kühn, J. G. and Patapis, P., "Active focal-plane coronagraphy with liquid-crystal spatial-light modulators: Broadband contrast performance in the visible," *Applied Optics* **61**, 9000–9009 (Oct. 2022).

[16] Eduardo E B, Guyon O, B. J., "Evaluation of spatial light modulator SLM for high contrast imaging." Evaluation of Spatial Light Modulator (SLM) for High Contrast Imaging https://www.jpl.nasa.gov/site/research/media/posters/2023/SP23006p.pdf. (Accessed: 2025-08-03).

[17] Riggs A J, Guyon O, B. J., "Evaluation of spatial light modulator SLM for high contrast imaging." Evaluation of Spatial Light Modulator (SLM) for High Contrast Imaging https://www.jpl.nasa.gov/site/research/media/posters/2024/SP23006p.pdf. (Accessed: 2025-08-03).

[18] Bordé, P. J. and Traub, W. A., "High-Contrast Imaging from Space: Speckle Nulling in a Low-Aberration Regime," *The Astrophysical Journal* **638**, 488 (Feb. 2006).